Supporting Information for

Relating Rates of Catalyst Sintering to the Disappearance of Individual Nanoparticles during Ostwald Ripening

Sivakumar R. Challa[1], Andrew T. Delariva[1,2], Thomas W. Hansen[1,2,3], Stig Helveg[2], Jens Sehested[2], Poul L. Hansen[2], Fernando Garzon[4] and Abhaya K. Datye[1,*]

[1]University of New Mexico, Albuquerque, New Mexico 87131, United States; [2]Haldor Topsøe A/S, Nymøllevej 55, DK-2800 Kgs. Lyngby, Denmark; [3]Center for Electron Nanoscopy, Technical University of Denmark, 2800 Kgs. Lyngby, Denmark; [4]Los Alamos National Laboratory, Los Alamos, New Mexico 87545, United States.

* email: datye@unm.edu

Catalyst Preparation and Pretreatments

For the experiments, a 12wt% Ni/MgAl$_2$O$_4$ steam reforming catalyst was used. In each experiment, a new specimen was prepared by simply "dipping" a plasma-cleaned stainless steel grid into the catalyst powder. The specimen was then mounted in a Gatan heating holder with an Inconel furnace. The Gatan holder was used due to its inertness to oxidizing conditions in the *in situ* TEM experiment. The sample temperature was measured with a PtRh thermocouple mounted on the furnace side and set using a Smartset controller. The TEM grid was held in place with a washer and screw also made from Inconel steel. Moreover the sample was sandwiched between two stainless steel grids with a lower mesh size in order to increase the radial heat transfer and reduce temperature non-uniformity. The two grids also provided better stability against thermal drift making it possible to image samples right after reaching the operating temperature.

The Ni particles were formed by H$_2$ reduction of the catalyst precursor for 30 minutes in 1.8mbar of H$_2$ at 500°C inside the microscope. Subsequently the samples were exposed to 3.6mbar 1:1 H$_2$:H$_2$O at 750°C. All temperature ramp rates were set to 50°C/min for consistency. The introduction of each gas was monitored by a mass spectrometer. The work described here focuses on the period when the sample had just reached the operating temperature (750°C) under 3.6 mbar H$_2$O:H$_2$, and for up to three hours after reaching this temperature.

Electron Microscopy

The measurements were done using a Philips CM300 FEG *in situ* TEM working at a primary electron energy of 300keV[1]. The microscope was fitted with a GIF2000 energy-loss spectroscopy system for both normal imaging and energy filtered imaging and a Tietz F114

camera for imaging at low electron doses. All images were obtained using the Tietz F114CCD camera and analyzed by using Digital Micrograph[TM] software. The images were calibrated and the image contrast and brightness was adjusted to improve the visibility of the Ni nanoparticles. Each particle contributing to the calculations and particle size distributions (PSD) was measured twice by hand from images using Digital Micrograph[TM] software, and the average of these measurements was used for further analysis. Approximately 200 particles were counted among all relevant samples to determine the PSD that is compared to simulations in Fig.3.

The microscope point resolution is 0.19 nm. Additionally, at the operating conditions, we could resolve 0.26-nm fringes in the oxide support, indicating at least a 0.26-nm resolution. However, fringes tended to fade in and out of contrast due to sample instability arising from the high temperature and the presence of gases. Hence, the particle size also shows variability from frame to frame.

The acquisition of time-lapsed TEM image series was done at a magnification corresponding to 0.2 nm/pixel. The image resolution was therefore 0.4-0.6 nm according to Nyquist's sampling theorem. The electron dose rate incident on the CCD was 74000 electrons/nm^{2}s over typical exposure times of 10 s, not including additional time for specimen area localization and image focusing. Single TEM images for particle size distribution were acquired of specific sample areas after reaching the desired temperature and after 30 min ageing under the *in situ* conditions. The corresponding images had an image pixel size of 0.08 nm/pixel and were acquired with a much lower electron dose rate incident on the CCD, again not including the time for specimen area localization and image focusing.

The movies were recorded with an image being collected every 50-500 milliseconds. Movie of ripening of a Ni nanoparticle captured in the *in situ* experiment is available on the web

(http://pubs.acs.org). Snapshots from this movie appear in Fig.1. The initial time ($t=0$) indicated in the plots of experimental data (Fig.2 and Fig.S7) is the time when imaging commenced after localization of the nanoparticles in the field of view and achieving stable imaging conditions. It is not the time when the experiment was initiated. Significant numbers of disappearances of small particles were observed as soon as the temperature in the *in situ* experiment reached the set temperature (750°C).[2]

The influence of the electron beam dose rate on the dynamics of particle disappearance was not investigated, but the agreement between the model predictions based on beam-on experiments and the observations in the beam-off experiments indicates that the impact of the electron beam on the observations is not significant.

Particle shape and size

The few particles identifiable in profile in Fig.1 indicate that their shape is close to being hemispherical. However, as reported elsewhere,[2] it was seen that there is a variation in the particle-support contact angle, θ, with smaller particles having a smaller contact angle. A variation of $50° < \theta < 130°$ would lead to K_{int} varying by a factor of 5.0-0.4, though it would be difficult and unwieldy to include a size-dependent θ in the ripening model being employed in the present work. So, a hemispherical assumption ($\theta = 90°$) may be considered reasonable.

The size of the particle refers to particle diameter. Each size measurement (for every image in the movie) involved drawing the longest chord. The movie was analyzed by three independent analysts. The size noted in Fig.2 is an average of the said three independent measurements.

Particle evaporation analysis

Langmuir was the first to derive an expression for evaluating rates of evaporation that was based on kinetic theory of gases.[3] Langmuir's equation refers to the evaporation of a metal from a flat surface into vacuum, to which we have added the Gibbs-Thomson equation, which is the exponential term in the following equation,

$$\frac{dr}{dt} = -\frac{p_0}{\rho}\sqrt{\frac{M_w}{2\pi R_g T}}\exp\left(\frac{2\gamma\Omega}{rk_b T}\right).$$

The vapor pressure, p_0, of Ni at 750°C is 6.94×10^{-10} Pa,[4] and the surface tension, γ, is 1.725 N/m.[5] The atomic volume, Ω, was obtained from the bulk density of Ni, $\rho = 8.9$ g/cm^3. Employing these values in the above relation and integrating numerically showed that a Ni particle of size 2.5 nm ($r = 1.25$ nm) would decrease to 2.497 nm in 30 minutes at 750°C in vacuum and that it would take ~130 hours for this particle to disappear completely (see Fig. S1). The shape of the predicted size-decay curve, though, is qualitatively similar to the observed decay of the Ni nanoparticle, with a relatively rapid decrease in size once the size diminishes to 1.5 nm. In the presence of H_2 and H_2O, even at as low a total pressure as 3.6 mbar, the predicted rate of evaporation would be much lower than the above maximum evaporation rate, since the atoms would undergo a diffusive transport process as explained by Fonda.[6] This is in contrast to evaporation in vacuum, which is much faster and is not impeded by the presence of gas atoms.
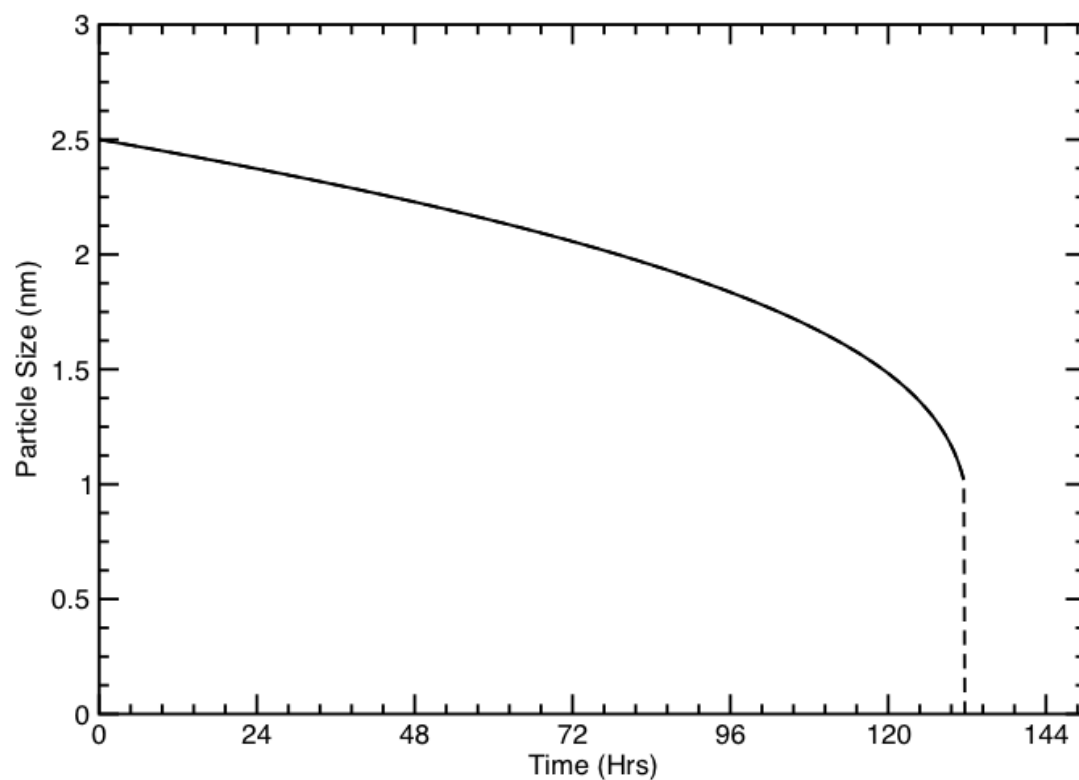
Figure S1. Size of a 2.5-nm Ni particle evaporating in vacuum at 750°C as predicted by Langmuir's model incorporating the Gibbs-Thomson (GT) relation. It would take >120 hr for a nanoparticle of this size to disappear by evaporation.
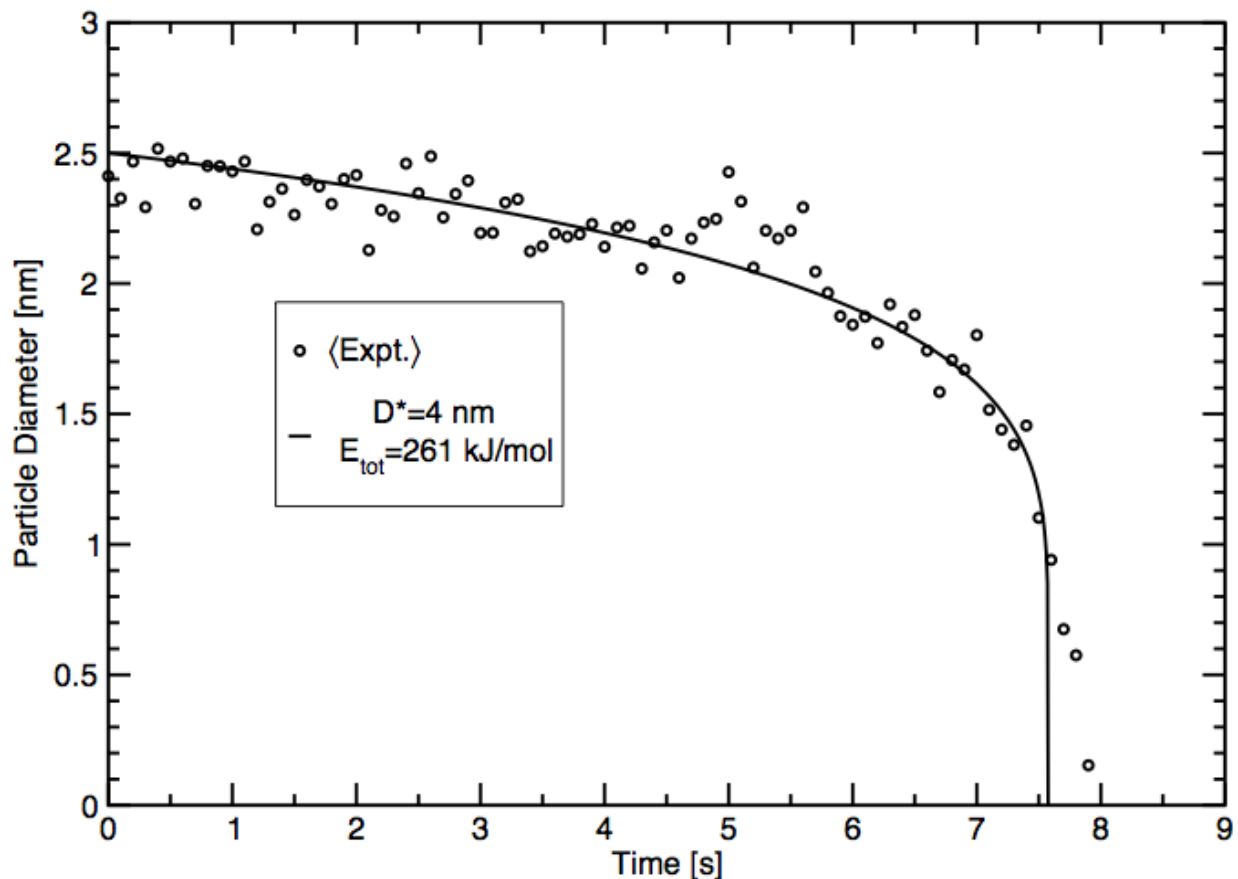
Figure S2. Size decay of a 2.5-nm particle as predicted by Eq. 3 that includes a finite value of r^* as observed in the *in situ* TEM experiment.

A parameterization of the experimentally observed size decay of a 2.5-nm Ni particle was presented in the main article. It is based on the simplified model (Eq. 4) and showed (Fig.1) an apparent activation energy of ripening (sintering) E_{tot} = 264.5 kJ/mol. A revised fit using a model that incorporates r^* (Eq. 3) is shown in Fig.S2. We used the smallest reasonable r^* so that the validity of our simplified model could be tested (d^* = 4 nm). The apparent energy of sintering is deduced to be E_{tot} = 261 kJ/mol. This is not much different from the parameterization based on Eq. 4, and is well within the range of E_{tot} employed in the sensitivity analysis (Fig.S4). Based on the actual initial size distribution of Ni nanoparticles the initial r^* was estimated to be d^* = 6 nm, implying that the prediction of size decay using this d^* would give rise to an activation energy of ripening 261<E_{tot}<264.5 kJ/mol. This further corroborates the use of Eq.4 based on the assumption that r<r^* for the parameterization of the Ni particle size decay data.
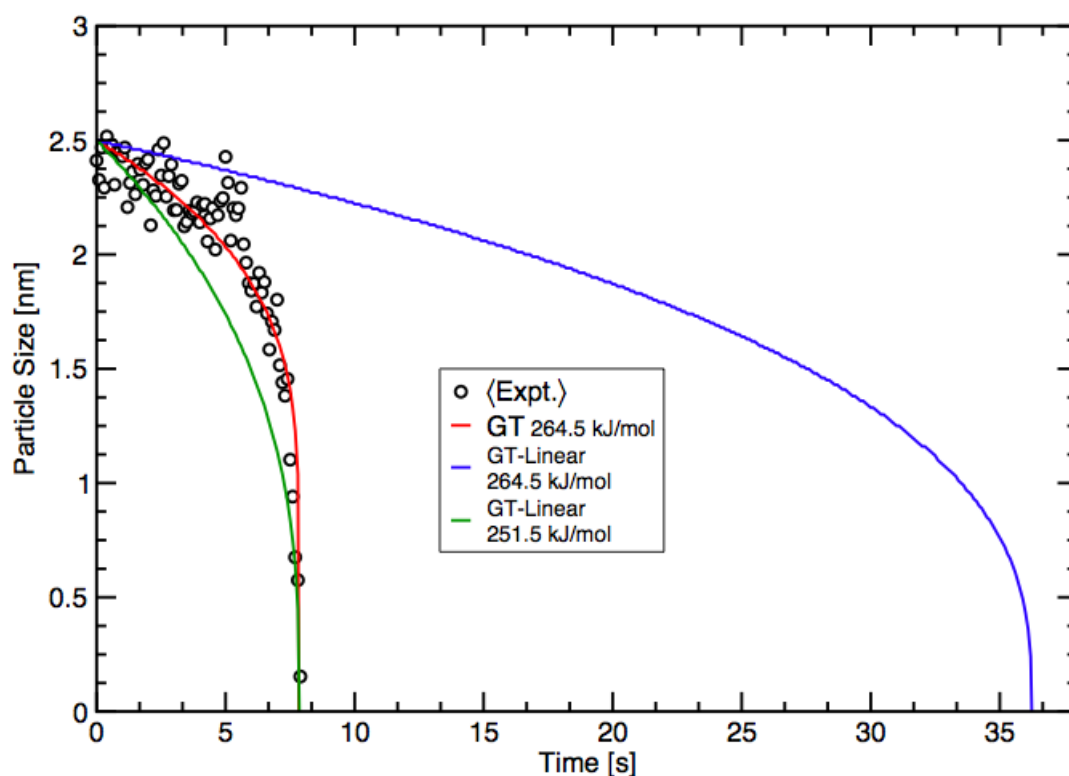
Figure S3. Comparison of predictions of size decay due to ripening: GT refers to ripening model incorporating complete Gibbs-Thompson relation, whereas GT-Linear refers to a linearized relation.

Figure S3 shows the predictions of size decay using the linearized GT relation in the Ostwald ripening model. The plots in the figure highlight two significant problems with the predictions based on a linearization. Employing K_{int} (or E_{tot}) from the fitting of size decay to the complete-GT ripening model leads to a large predicted lifetime for the 2.5-nm Ni particle (>35 s). Even a best-fit for the linearized model that matches the experimental lifetime of the 2.5-nm nanoparticle does not provide good agreement with the decay is size observed experimentally.
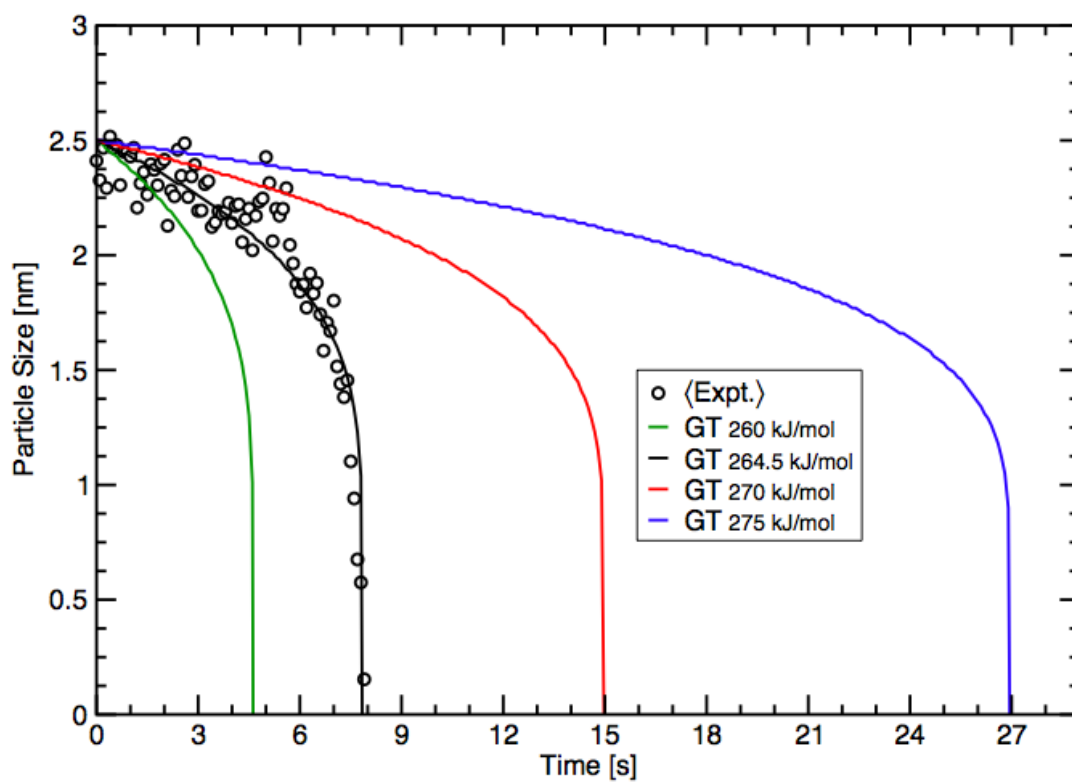
Figure S4. Sensitivity analysis of Eq.4 with different K_{int} values showing the predicted variations in the particle lifetime of a 2.5-nm Ni particle.
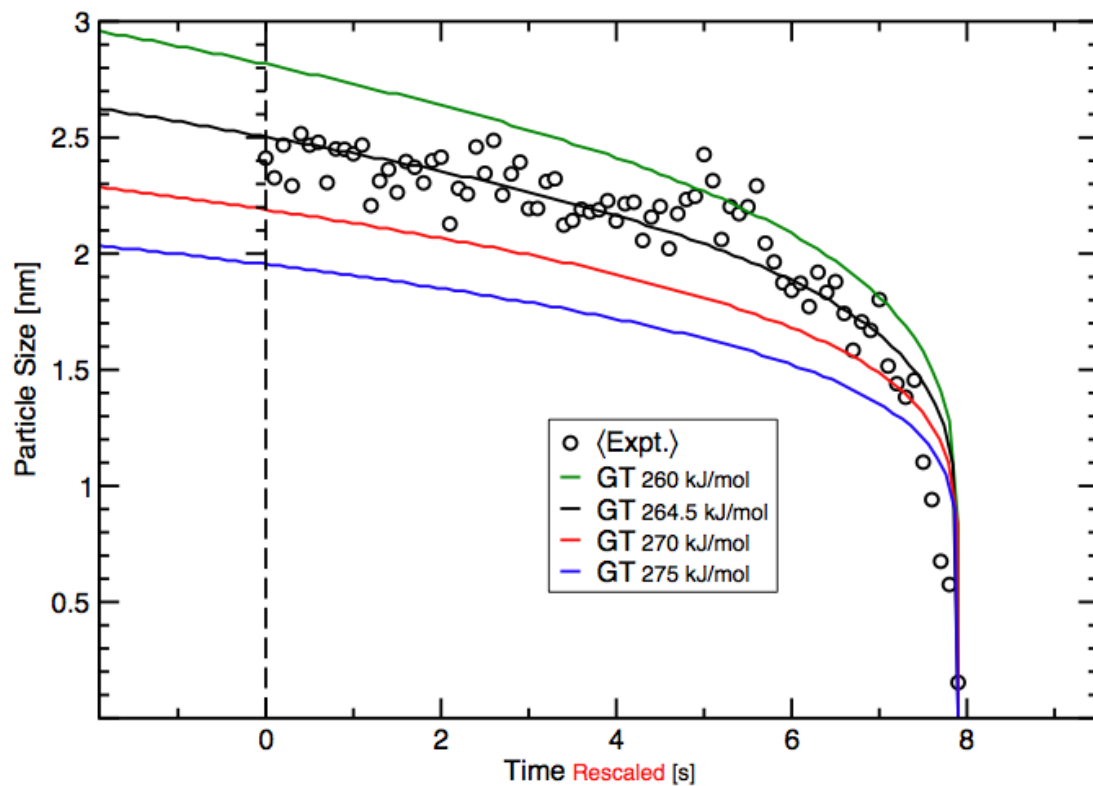
Figure S5. Sensitivity analysis of Eq.4 with different K_{int} values showing the predicted variations in the initial particle size. The predicted curves are translated (rescaled) to have a common time-of-disappearance, otherwise the same data as in Fig. S4.
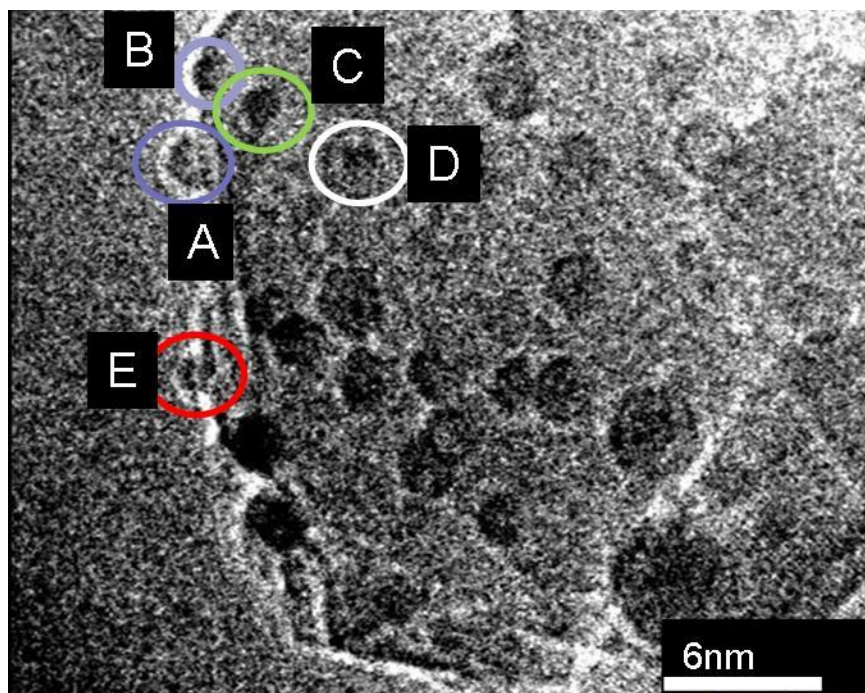
Figure S6. Five Ni particles supported on MgAl$_2$O$_4$ that underwent ripening at 750°C.
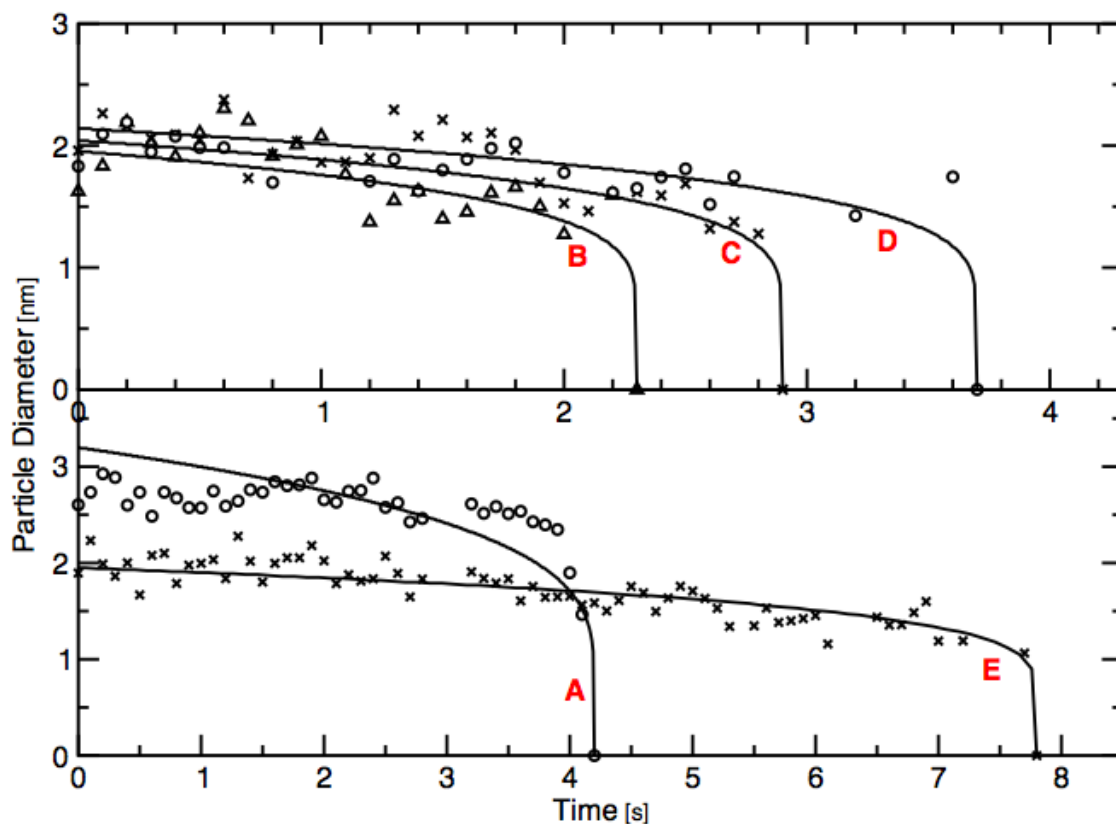
Figure S7. Predicted size decay of several Ni particles (highlighted in Fig.S6) as predicted by Eq.4: (top) using $E_{tot} = 264.5$ kJ/mol, and (bottom) using different $E_{tot} = 275$ kJ/mol (circles) and 250 kJ/mol (crosses). The alphabets correspond to highlighted particles in Fig.S6.

The size of several other Ni particles in the same *in situ* experiment was extracted in the same way. The estimated E_{tot} (= 264.5 kJ/mol) for the 2.5-nm particle was found to fit very well for three other particles. However, for two other particles, the best fit of Eq. 3 was obtained with a slightly different E_{tot}, close to the variation of ±5-10 kJ/mol pointed out in the sensitivity analysis. This variation in E_{tot} may be attributed to variations in the substrate or to local effects (different numbers of neighboring particles), though sufficient data is lacking to make conclusive statements. Such effects may also explain why the observed size decay in the lower display for the smaller particle is slower than for the larger particle.

Complete references

(3) Datye, A. K.; Xu, Q.; Kharas, K. C.; McCarty, J. M. *Catal. Today* **2006**, 111, 59-67.

(4) Xu, Q.; Kharas, K. C.; Croley, B. J.; Datye, A. K. Chem. Cat. Chem, 2011, 6, 1004-1014.

(6) Sehested, J.; Carlsson, A.; Janssens, T. V. W.; Hansen, P. L.; Datye, A. K. J. Catal. 2001, 197, 200-209.

(7a) Borup R.; Meyers, J.; Pivovar, B.; Kim, Y. S.; Mukundan, R.; Garland, N.;Myers, D.; Wilson, M.; Garzon, F.; Wood, D.; Zelenay, P.; More, K.; Stroh, K.; Zawodzinski, T.; Boncella, J.; McGrath, J. E.; Inaba, M.; Miyatake, K.; Hori, M.; Ota, K.; Ogumi, Z.; Miyata, S.; Nishikata, A.; Siroma, Z.; Uchimoto, Y.; Yasuda, K.; Kimijima, K.-I.; Iwashita, N. *Chem. Rev.* **2007**, *107*, 3904-3951.

(7b) Mayrhofer, K. J. J.; Ashton, S. J.; Meier, J. C.; Wiberg, G. K. H.; Hanzlik, M.; Arenz, M. J. Power Sources 2008, 185, 734-739.

(9) Sambles, J. R.; Skinner, L. M.; Lisgarten, N. D. Proc. R. Soc. Lond. A. 1970, 318, 507-522.

(10) Yang, F.; Chen, M. S.; Goodman, D. W. J. Phys. Chem. C 2009, 113, 254-260.

(11) Simonsen, S. B.; Chorkendorff, I.; Dahl, S.; Skoglundh, M.; Sehested, J.; Helveg, S. J. Am. Chem. Soc. 2010, 132, 7968-7975.

(13) Sehested, J.; Gelten, J. A. P.; Remediakis, I. N.; Bengaard, H.; Nørskov, J. K. J. Catal. 2004, 223, 432-443.

(14a) Baker, R. T. K.; Harris, P. S.; Thomas, R. B. Surf. Sci. 1974, 46, 311-316.

(14b) Liu, R.-J.; Crozier, P. A.; Smith, C. M.; Hucul, D. A.; Blackson, J.; Salaita, G. Appl. Catal. A 2005, 282, 111-121

(20a) Meyer, R.; Ge, Q.; Lockemeyer, J.; Yeates, R.; Lemanski, M.; Reinalda, D., Neurock, M. Surf. Sci. 2007, 601, 134-145.

(20b) Deskins, N. A.; Mei, D.; Dupuis M. Surf. Sci. 2009, 603, 2793-2807.

(20c) Valero, M. C.; Raybaud, P.; Sautet, P. Phys. Rev. B 2007, 75, 045427.

(23a) Morgenstern, K.; Rosenfeld, G.; Comsa, G. Phys. Rev. Lett. 1996, 76, 2113-2116.

(23b) Bartelt, N. C.; Theis, W.; Tromp, R. M. Phys. Rev. B 1996, 54, 11741-11751.

(25) Houk, L. R.; Challa, S. R.; Grayson, B.; Fanson, P.; Datye, A. K. Langmuir 2009, 25, 11225-11227.

(26) (a) Luo, W.; Hu, W.; Xiao, S. J. Phys. Chem C 2008, 112, 2359-2369.

References

1. P. L. Hansen, S. Helveg, A. K. Datye, *Adv. Catal.* **2006**, *50*, 77-95..
2. A. Delariva, Ph.D. Dissertation, University of New Mexico, Albuquerque, NM, 2010.
3. I. Langmuir, *Phys. Rev.* **1913**, *2*, 329-342.
4. *CRC Handbook of Chemistry and Physics*, Internet ed.; D. R. Lide, Ed.; CRC Press: Boca Raton, FL, 2005.
5. *CRC Handbook of Materials Science Vol.I General Properties*, C. T. Lynch, Ed.; CRC Press: Boca Raton, FL 1986.
6. G. R. Fonda, *Phys. Rev.* **1923**, *21*, 343-347.